Turkish Journal of Electrical Engineering & Computer Sciences

http://journals.tubitak.gov.tr/elektrik/

Research Article

Turk J Elec Eng & Comp Sci
(2021) 29: 2046 – 2066

doi:10.3906/elk-2008-164

Legendre-wavelet embedded NeuroFuzzy feedback linearization based control scheme for PHEVs charging station in a microgrid

Muhammad AWAIS[1], **Laiq KHAN**[2,*], **Saghir AHMAD**[1], **Sidra MUMTAZ**[1], **Rabiah BADAR**[2], **Shafaat ULLAH**[1]

[1]Department of Electrical and Computer Engineering, COMSATS University Islamabad, Abbottabad, Pakistan
[2]Department of Electrical and Computer Engineering, COMSATS University Islamabad, Islamabad, Pakistan

Received: 31.08.2020 • **Accepted/Published Online:** 29.04.2021 • **Final Version:** 26.07.2021

Abstract: The immense emergence of plug-in hybrid electric vehicles (PHEVs) is envisioned in the future. The rapid proliferation of PHEVs and their charging triggers intense surges in the load during load peak hours. A sophisticated controlled charging station is developed for PHEVs to alleviate grid load during peak demand hours. A novel feedback linearization embedded full recurrent adaptive NeuroFuzzy Legendre wavelet control (FBL-FRANF-Leg-WC) technique is employed to control the charging of PHEVs. The antecedent part of the NeuroFuzzy framework is based on recurrent Gaussian membership function while the consequent part comprises of recurrent Legendre wavelet. The charging station is integrated into a grid-connected microgrid hybrid power system. The charging station consists of five different PHEVs with seven different modes of operation. The performance of the control scheme is tested for various power quality and power system stability parameters. The effectiveness of the suggested control scheme is validated through simulation results by comparing with adaptive NeuroFuzzy, adaptive PID, and conventional PID control scheme.

Key words: Smart microgrid hybrid power system (SMG-HPS), plug-in hybrid electrical vehicle (PHEV), maximum power point tracking (MPPT), charging station (CS), feedback linearization (FBL), NeurFuzzy (NF), recurrent, legendre wavelet

Nomenclature

Control schemes parameters		Abbreviations	
m_{ij}	mean of ith input and jth membership function	RES	renewable energy resources
σ_{ij}	variance of ith input and jth membership function	PHEV	plug-in hybrid electrical vehicle
μ_{ij}	membership function	MG	microgrid
H_i	output of hidden layer	HPS	hybrid power system
F_i	feedback weight of consequent part	CS	charging station
β_{ij}	output of consequent part	PV	photovoltaic
γ	cost function	UG	utility grid
θ_i	recurrent weight of antecedent part	FRANF	full recurrent adaptive NeuroFuzzy
n_s	number of series panels	ANN	artificial neural network
Abbreviations		SMG	smart microgrid
FBL	feedback linearization	NF	NeuroFuzzy

*Correspondence: laiqkhan@comsats.edu.pk

1. Introduction

Today's society is facing a shortage of energy and mainly depends on fossil fuels to fulfill energy demand. Increasing cost, high carbon emission rate, pollution issues, global warming, and limitation of supplies are some critical problems related to the use of fossil fuels to produce energy [1–6]. These challenges can be contained by sustainable consumption, efficient transformation of energy from one kind to another, and focusing on new cost-effective, clean, and green non-conventional renewable energy resources (RES) instead of conventional non-renewable energy resources [1, 7, 8].

The study and analysis of the energy demand of the globe have forced the engineers, scientists, and companies to go for a never-ending search for sustainable energy. This search for sustainable energy is proceeding in a specific way where it always tries not only to meet the ever-increasing demand for energy but focuses on keeping the environment in its original form. The leading energy consumer automobile industry is growing exponentially and is one of the main contributors to environmental issues. The estimate of greenhouse emission from the transportation sector compels stakeholders to invest in the research and development of sustainable and fuel-efficient transportation systems that reduce and replace conventionally non-renewable, fossil fuel-based energy resources with that of RES [1, 7].

Plug-in hybrid electrical vehicles (PHEVs) consume electrical energy from the electrical grid. However, they can be operated only on electric power in urban localities; thus, they give zero-emission and contribute to a safer environment. However, large-scale integration of PHEVs creates potential problems and advantages for the grid. The critical impact of a large number of PHEVs integration on the electric grid is the increase in peak demand that may lead to a destabilized performance and fluctuations in electric energy on the overall electrical power system. On the other hand, charging and discharging of PHEVs act as an elastic load and benefit the grid by shaping the load profile [9].

In recent years, smart micro-grid hybrid power system (SMG-HPS) technology integrated with RES has been developed, which provides clean energy to the electrical power system and encourage the use of PHEVs. The natural abundance of wind and photovoltaic (PV) on the earth makes them first as RES. Both wind and PV depend on weather conditions, which gives variable output power [10]. This property of RES requires the integration of energy storage systems in SMG-HPS. The bidirectional power flow between the electric grid and the PHEV charging station (CS) integrated into the SMG-HPS ultimately enhances the power reliability of SMG-HPS. However, a suitable control algorithm and appropriate energy management system are required for reliable performance of CS and creates new room for research [3, 11–13]. In CS, the unpredictable number of PHEVs and their energy demand can create instability in transmission and distribution systems especially during peak hours [14]. Thus, a comprehensive control scheme is required to enhance SMG-HPS power system stability.

Two types of techniques are in practice for PHEV's charging. A unidirectional power flow technique known as an uncoordinated technique in which PHEVs are charged directly from the utility grid till their maximum state of charge (SOC) limit reaches. However, in this technique, PHEV's act as a simple load that destabilizes the electric grid during peak hours and causes power quality issues. On the other hand, a bidirectional power flow technique known as a coordinated technique is also in practice and is preferred over uncoordinated technique due to its capability of grid support in terms of power back up during peak hours. Other benefits of coordinated technique include the reduction in SMG-HPS operational cost, high reliability of SMG-HPS, and the frequency regulation [3, 15–17].

In literature, many articles are presented regarding the control of PHEVs charging/discharging via

CS, connected with RES or grid and their impact on the overall electrical power system. [12, 18] presents a PI control, [19] explored dynamic, and quadratic programming based control method, [5] presents the quadratic optimization scheme, [20] describes linear programming, and [21] gives linear programming based charging/discharging control of PHEVs. All these techniques are conventional control techniques intended for specific operating conditions and are not suitable for a wide-range of varying system conditions [3]. [13] studies fuzzy logic (FL) control scheme for PHEV charging/discharging through RES, while [11] describes scheduling of PHEVs charging/discharging phenomena based on microgrid's day-a-head load curves using FL and artificial neural network (ANN) and [10] describe day-ahead optimization of prosumer using feed-forward ANN. However, FL has problems with exponential growth in the number of membership functions and if-then rules. It needs to be redefined whenever the system parameters change; whereas, ANN requires periodic training for its convergence [15, 22].

In [9] the author describes a novel scheme for charging/discharging of PHEVs based on peer-to-peer communication between charging stations. However, the scheme lacks practical considerations of the electrical power system. In [23] an equivalent consumption minimization strategy is described and the forthcoming energy consumption prediction for all-electric range. However, the optimization technique requires certain assumed constraints and an ideal environment for its application. Also application of particle swarm optimization and ANN for optimization and prediction makes it complex and bulky. In [16], the author presents multiple model predictive control for charging/discharging of PHEVs and microgrid frequency stabilization. However, the control scheme has difficulties with the operation, high maintenance cost, and lack of flexibility. [3, 24] practices adaptive PID (aPID) control for charging/discharging of PHEVs connected to HPS. However, aPID suffers performance loss in the varying environment and cannot deal well with large systems as presented.

This paper demonstrates a feedback linearization embedded full recurrent adaptive NeuroFuzzy Legendre wavelet control (FBL-FRANF-Leg-WC) technique for bidirectional charging/discharging of PHEVs in a CS connected to an SMG-HPS. The grid-connected SMG-HPS has several RES and other sources for power generation. The bidirectional charging/discharging is taken for seven different scenarios. Gaussian function and Leg-wavelet is used to approximate the nonlinear functions of FBL control through full recurrent adaptive NeuroFuzzy structure having seven-layers. The gradient-descent method is used for online learning to update adaptive parameters of FRANF structure. The performance of the suggested control scheme is compared against adaptive NF, conventional PID, and aPID control schemes for charging/discharging of PHEVs, AC-bus active and reactive power, %SOC of PHEVs, active and reactive power of CS's inverter, total harmonic distortion (THD), voltage, and frequency fluctuations on the load side.

After the introduction in Section 1 the article is arranged as follows: Section 2 presents the complete details of microgrid hybrid power system and charging station used for this investigation. Section 3 explains the proposed closed-loop adaptive FBL-FRANF-Leg-WC scheme for CS. Section 4 provides the detail of computer simulation studies and CS operation modes. Section 5 discusses the simulation results. Finally, Section 6 concludes the findings of this research work.

2. Microgrid hybrid power system and charging station subsystem

A schematic of the overall proposed MG-HPS is illustrated in Figure 1. It includes a DC-bus and an AC-bus, which are interconnected via the main inverter. All RES like electrolyzer, wind-turbine (WT), solid oxide fuel cell (SOFC), PV, super-capacitor (SC), and batteries are connected to a DC-bus. While other power sources

like utility grid (UG) and micro-turbine (MT) are connected to AC-bus. All the loads are connected to AC-bus. A CS capable of bidirectional charging/discharging acts as load as well as source is also connected to AC-bus. The power rating of all the sources is given in Table 1 [22]. Other details of SMG-HPS control, solar profile, etc., are given in [22]. aPID is used to control all source converters except CS. Table 2 gives the detail of PHEV's batteries [3, 24].

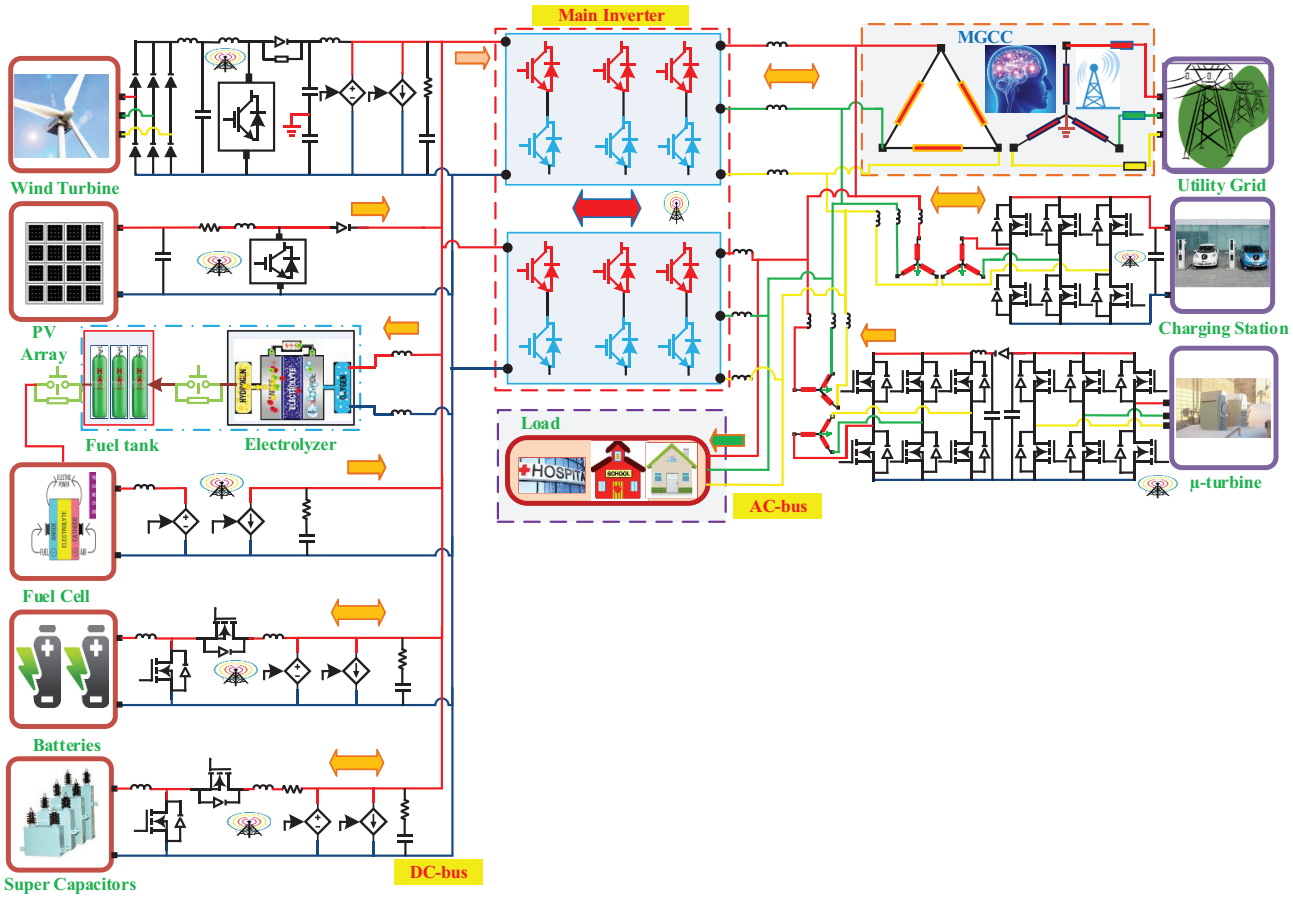

Figure 1. Schematic of microgrid hybrid power system.

3. Adaptive feedback linearization embedded full recurrent adaptive Neurofuzzy legendre wavelet control for charging station

Figure 2 shows the internal structure and control scheme of the CS. It consists of a battery storage system (BSS) and five different PHEV models. Table 2 shows the detail of PHEV's battery used for this research work. Each PHEV and BSS are connected with a buck-boost converter and a voltage regulator. Buck-boost converters are controlled by aPID controllers for buck mode and boost mode of operation, respectively. Adaptive FBL embedded FRANF-Leg-WC is used to control the voltage regulator.

FBL is a technique that converts the nonlinear dynamics of the system into linear dynamics algebraically, partly or fully; thus, linear control scheme can be applied easily [22]. Consider a nonlinear system:

$$y^n = f(x) + g(x)u_{PHEV} \tag{1}$$

Table 1. Parameters of the microgrid system.

Source	Rating
UG	11 kV
PV	260 kW
WT	100 kW
Electrolyzer	150 kW
SOFC	260 kW
MT	200 kVA
SC	165 F
Batteries	200 Ah

Table 2. Parameters of PHEV's batteries.

Vehicle Company	Battery Type	Battery Capacity (kWh)	Rated Voltage (V)
Nissan	Li-ion	24.0	360
Renault	Li-ion	22.0	300
Mitsubishi	Li-ion	16.0	20
Toyota	Li-ion	6.7	300
Honda	Li-ion	4.4	201

Where $y \in \Re$ is the plant output, *f(x)* and *g(x)* are the unknown nonlinear functions, $n \in \mathbb{Z}$ is the relative degree of system, $u_{PHEV} \in \Re$ is the control input, and $x = [y, \dot{y}, , y^{n-1})]^T \in \Re^n$ is the state-space vector. The control objective is to find u_{PHEV} that forces $y(t)$ to follow the desired trajectory $y_d(t)$. The error matrix e is:

$$e = y(t) - y_d(t) \tag{2}$$

The tracking error κ is given as [22]:

$$\kappa^T = \begin{bmatrix} \wr^T & 1 \end{bmatrix} e \tag{3}$$

Where $\wr = \begin{bmatrix} \vee_1 & \vee_2 & \cdots & \vee_{n-1} \end{bmatrix}$ is the weight vector of FBL whose approximate choice ensures that poles of $s^{n-1} + \vee_{n-1} s^{n-2} + \cdots + \vee_1$ in the left half of complex plane and e is given in (2). $\wr$ is updated at every step using nLMS self-tuning algorithm. The derivative of (3) is:

$$\dot{\kappa}^T = \begin{bmatrix} \wr^T & 1 \end{bmatrix} \dot{e} = \begin{bmatrix} \wr^T & 1 \end{bmatrix} (\dot{y}_d(t) - \dot{y}(t)) = [y^n]^T + [-y_d^n]^T + \begin{bmatrix} 0 & \wr^T \end{bmatrix} e = y^n + \kappa_D^T \in \Re^{1 \times n} \tag{4}$$

Using (1) in (4):

$$\dot{\kappa} = f(x) + g(x) u_{PHEV} + \kappa_D \tag{5}$$

Using $\kappa = exp(-\Xi t) \Rightarrow \dot{\kappa} = -\Xi\kappa$ and constant $\Xi > 0$, if κ is considered as input in (3) and e as output, then

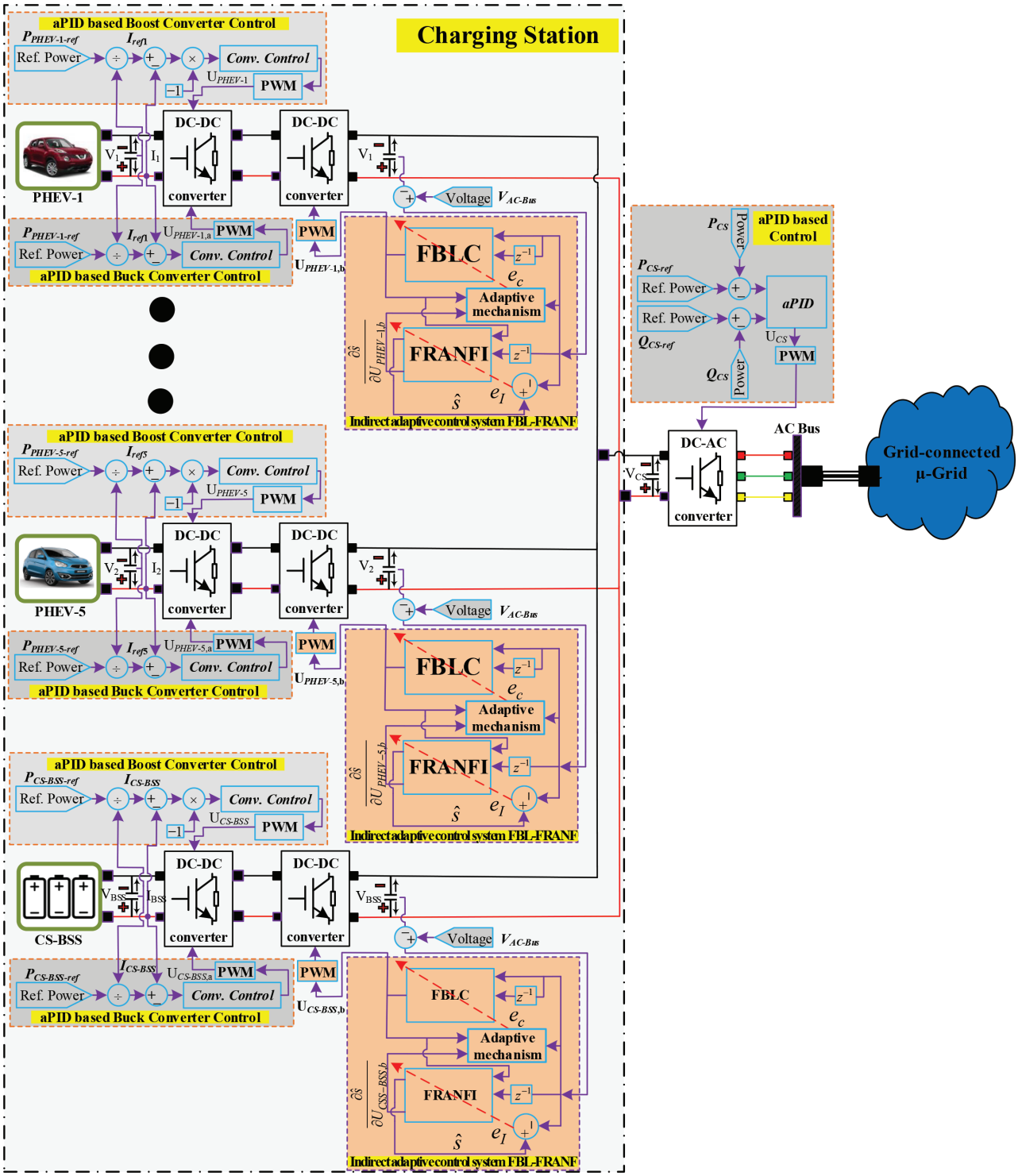

Figure 2. Closed-loop control of plug-in hybrid electric vehicles.

$e \to 0$ as $\kappa \to 0$. (5) can be rewritten as:

$$-\Xi\kappa = f(x) + g(x)u_{PHEV} + \kappa_D \tag{6}$$

Now, if the nonlinear functions $f(x)$ and $g(x)$ are known, then according to the FBL mechanism the following control law u_{PHEV} can be obtained that can revoke the nonlinearities of the system and would bring κ to zero.

$$u_{PHEV} = \frac{1}{g(x)}\left[-f(x) + \Xi\kappa + \kappa_D\right] \tag{7}$$

However, identification of $f(x)$ and $g(x)$ is necessary for the implementation of the above control law. Therefore, this study proposes the estimation of nonlinear functions $\widehat{f}(x)$ and $\widehat{g}(x)$ through FRANF-Leg-WC for online optimization of design parameters $\wr$. (7) can be rewritten as:

$$u_{PHEV} = \frac{1}{\widehat{g}(x)}\left[-\widehat{f}(x) + \Xi\kappa + \kappa_D\right] \tag{8}$$

For the best approximation of $\widehat{f}(x)$ and $\widehat{g}(x)$ in (8), a seven layer FRANF-Leg-WC is used in this research work as shown in Figure 3 [22]. The inputs to the FRANF-Leg-WC is the difference between the output voltage of PHEVs voltage regulator and AC-bus voltage. The output of FRANF-Leg-WC are estimated nonlinear functions $\widehat{f}(x)$ and $\widehat{g}(x)$. Mean square error (MSE) is used as a cost function to update the parameters of the antecedent and the consequent parts as given in equation (9):

$$E = \frac{1}{2}(\widehat{y} - y)^2 \tag{9}$$

Where, $\widehat{y} = \widehat{f}(x) + \widehat{g}(x)u_{PHEV}$ and $y = V_{PHEV}$. For fast convergence, gradient descent method is used as follows:

$$\wp(m+1) = \wp(m) - \Gamma\varrho_m \tag{10}$$

Where, ϱ_m is the gradient of the cost function at mth iteration, $\Gamma > 0$ is the learning rate and m is the iteration index. The gaussian membership function is used for antecedent part of FRANF and is given below:

$$O_i^{(2)} = \mu_j(x_i) = exp\left[-\left(\frac{x_i(k) + \mu_j(k-1)\theta_{ij} + m_{ij}}{\sigma_{ij}}\right)^2\right] \tag{11}$$

Where O_i represents output of ith node, superscript (2) indicates layer number, ij subscript shows the jth term of the ith input, x_i is the input, $\mu_j(k-1)$ is the past value of membership function, θ_{ij} is the recurrent weight, σ_{ij}, and m_{ij} are the variance and mean of the ith input and jth membership function.

Legendre wavelet (Leg-W) is used as a variant of the consequent part in this research work. These are also known as spherical harmonic wavelets. They are based on Legendre polynomial, compactly supported, and orthonormal wavelets. They can be expressed as [25]:

$$\Psi_{pq}^k(x) = \begin{cases} 2^{p+1}\sqrt{2k+1}L_k\left(2^p x - q - 0.5\right), & \forall \frac{q}{2^p} \le x \le \frac{q+1}{2^p} \\ 0, & otherwise \end{cases} \tag{12}$$

Where, $p = 1, 2, ...m$ and $q = 0, 1, ...2^p - 1$ shows decomposition level and integer translation, respectively. L_k shows the Legendre polynomial as given in (13), with k being the degree of the polynomial [25].

$$L_p(x) = \frac{1}{2^p n!}\frac{d^n}{dx^n}\left(x^2 - 1\right)^p \tag{13}$$

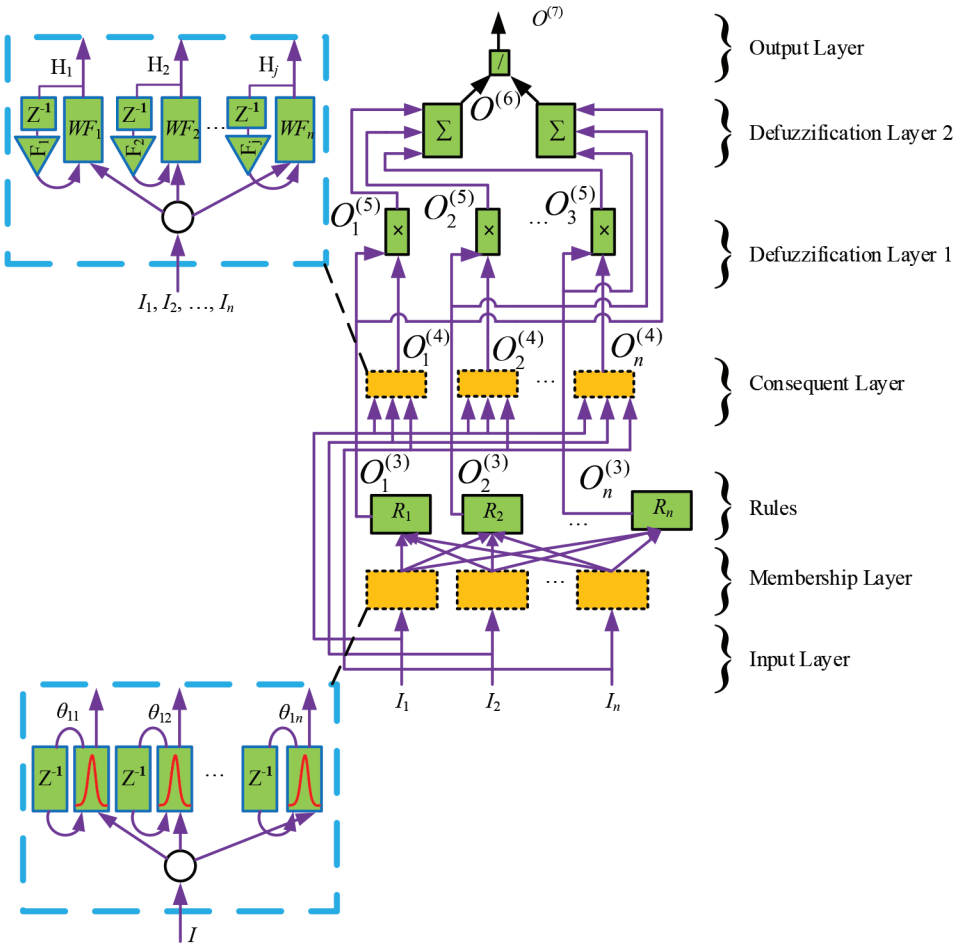

Figure 3. Architecture of full recurrent adaptive NeuroFuzzy system.

Where, $p \geq 0, x \in [-1 \;\; 1]$. The first four Legendre polynomials for $p = 0, ..., 3$ used in this work are given below [25]:

$$L_o(x) = 1, L_1(x) = x, L_2(x) = 0.5\left(3x^2 - 1\right), L_3(x) = 0.5\left(5x^3 - 3x\right). \tag{14}$$

Six Leg-W basis functions are used in this research work for $p = 1$ and $i = 0, ..., 2$ defined on $[0 \;\; 1]$.

The signal propagation and operation function of nodes in each layer is given as under:

Layer 1: This layer receives input signals and transmit them to the next layer and have feedback connections that add temporal relationship in-network. The output of this layer is: $O_i^{(1)} = I_i$.

Layer 2: This layer estimates membership degree and fuzzy set for all inputs using Gaussian membership function according to (11).

Layer 3: This layer is also known as rule layer and gives product of membership functions. The number of rules in this layer determines the number of nodes where each node corresponds to a fuzzy rule. The output

of this layer is as follows:

$$O_i^{(3)} = \prod_{i=1}^{n} \mu_j = \prod_{i=1}^{n} exp\left[-\left(\frac{x_i + \mu_i(k-1)\theta_{ij} - m_{ij}}{\sigma_{ij}} \right)^2 \right] \tag{15}$$

Layer 4: The consequent nodes compute the weighted firing strength of the rule layer and represent THEN-part of fuzzy rules. The input to this layer is the error signal and weighted feedback signal of the same layer. The output of this layer is given below:

$$O_i^{(4)} == H_i(k) + F_i H_i(k-1) \tag{16}$$

Where, $H_i = \sum_{p=1}^{N} \sum_{q=0}^{2^p-1} \sum_{k=0}^{K} w_{nm}^k \Psi_{pq}^{(k)}$, w_{nm} represents Legendre wavelet coefficients, and F_i is the feedback weight. It is noteworthy that feedback weight of this layer is not adaptive but a closed loop fixed gain.

Layer 5: The first defuzzification layer produces sum of products of antecedent and consequent parts of (15) and (16). The output of this layer is given below:

$$O_i^{(5)} = \sum_{i=1}^{n} O_i^{(4)} O_i^{(3)} \tag{17}$$

Layer 6: The second defuzzification layer computes the sum of all the rules from equation (15). The output of this layer is given below:

$$O_i^{(6)} = \sum_{i=1}^{n} Oi^{(3)} \tag{18}$$

Layer 7: The output layer gives the approximated nonlinear functions at its output. The output of this layer is given below:

$$O_f^{(7)} = \widehat{f}(x) = \frac{O_{fi}^{(5)}}{O_{fi}^{(6)}} \tag{19}$$

$$O_g^{(7)} = \widehat{g}(x) = \frac{O_{gi}^{(5)}}{O_{gi}^{(6)}} \tag{20}$$

The update equations and other details of FRANF are given in [22].

4. Computer simulation studies

The performance of SMG-HPS and CS is evaluated with proposed adaptive FBL embedded FRANF-Leg-WC, adaptive NF, aPID and PID in Matlab/Simulink R2015a. The details of MG-HPS are given in Table 1. The ambient temperature (^{o}C), solar irradiation (W$/m^2$), and wind speed (m/s) are obtained from Pakistan Meteorological Department (PMD) for a complete solar day at Islamabad station. The solar irradiance and wind speed are shown in Figure 4. The converters installed at the charging station are responsible for bidirectional charging and discharging. Bidirectional power flow between UG and CS takes place via the converter of CS and is useful for various modes of operations described in Section 4.1.

The simulation result are obtained for the power quality and power system stability parameters, like oscillations in active/reactive bus-power, $\%\Delta$THD, $\%\Delta V_{RMS}$, and $\%\Delta$f. These results are explained in the Section 5 in detail.

4.1. Modes of charging station operation

Figure 5 shows the proposed modes of operation for CS. Seven modes of operation are considered to test the reliability of the proposed model. These modes include V2G, G2V, BSS2G, G2BSS, V2BSS, BSS2V, and V2V.
Mode 1 (V2G): Peak time is considered in this mode of operation where PHEV and BSS have energy stored

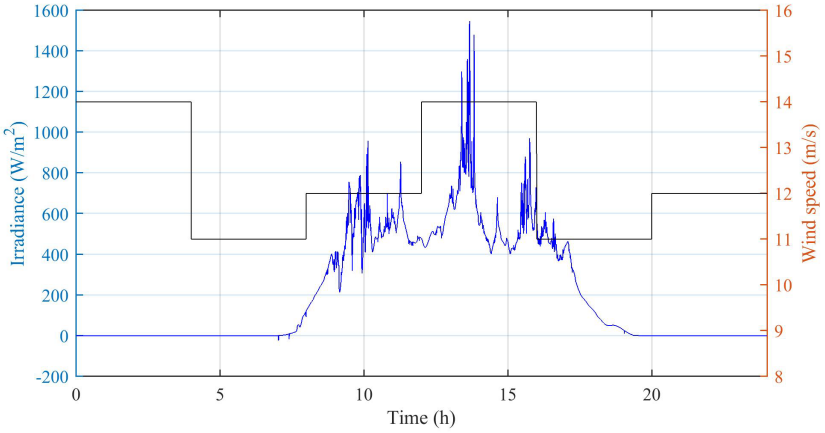

Figure 4. Solar irradiance and wind speed.

in them while UG needs power, which flows from CS to the grid.
Mode 2 (G2V): In this mode of operation PHEV needs power due to low SOC and obtain power from the AC-bus.
Mode 3 (BSS2G): It is similar to V2G mode of operation but in this mode, BSS is discharging instead of PHEV and provides power to UG during peak hours.
Mode 4 (G2BSS): In this mode, BSS has a low SOC and is in charging mode thus UG is providing power to BSS.
Mode 5 (V2BSS): In this mode, PHEV is providing power to BSS.
Mode 6 (BSS2V): In this mode, BSS is providing power to PHEV.
Mode 7 (V2V): In this mode, PHEV is providing power to another PHEV.
Figure 6 shows an energy management system for all the modes of operation of CS.

5. Results and discussion

The simulation results of the proposed control scheme are compared with adaptive NF, conventional aPID and PID control schemes. The detailed discussion is given below:
Figure 7 and Figure 8 show the active and reactive power of AC-bus. The results reveal different modes of operation during peak load time as well as valley time on power profile. The UG power absorbs power from CS during peak hours and delivers power to CS to meet its power demand. It is clear from Figure 7 and Figure 8 that the proposed adaptive FBL embedded FRANF-Leg-WC tracks the reference active and the reactive power of AC-bus more efficiently as compared with adaptive NF, aPID and PID control schemes.

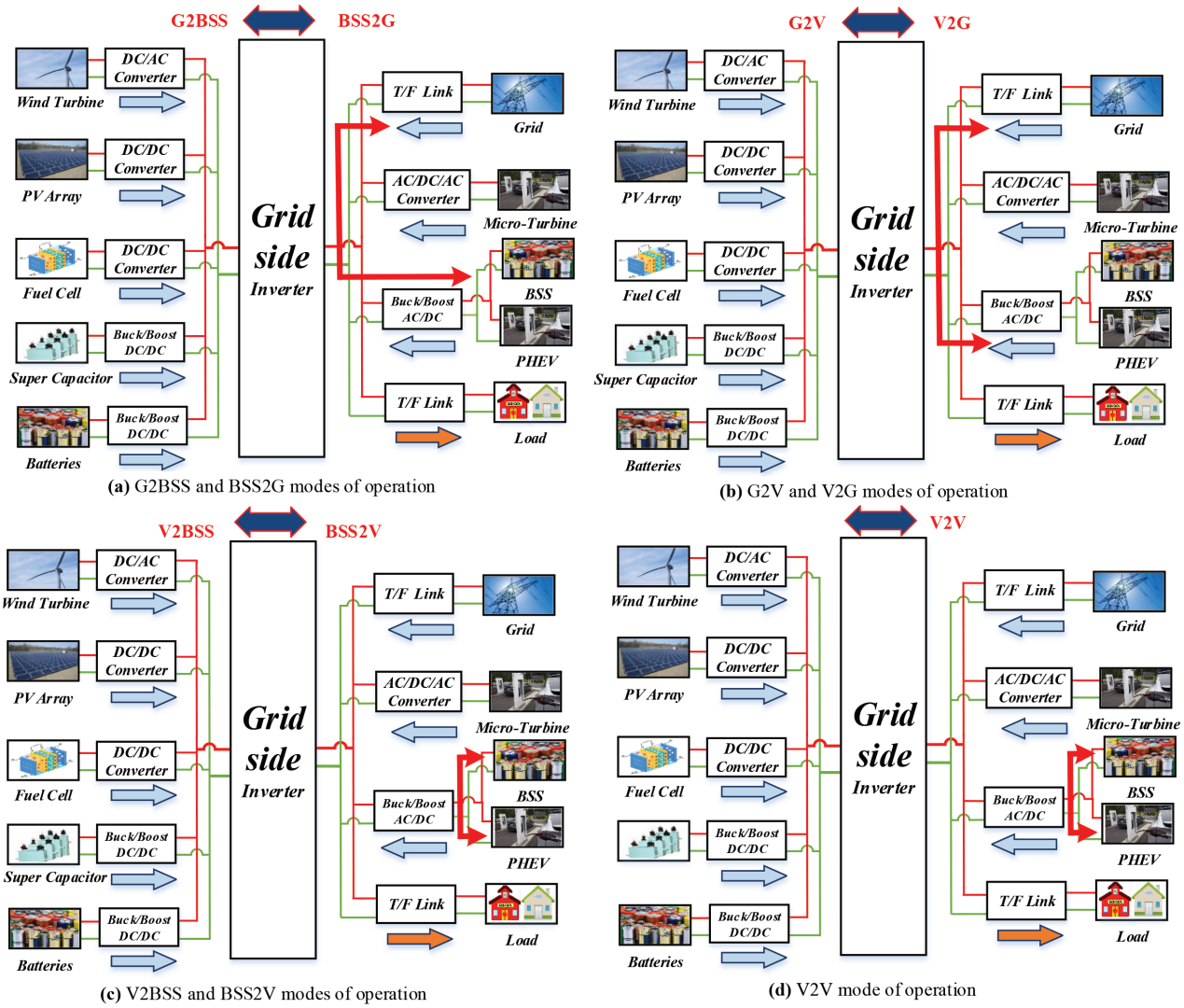

Figure 5. Operational modes of charging station.

The converter of CS is responsible for bidirectional charging/discharging and all the seven proposed modes of operation in Section 4.1. Figure 9 and Figure 10 show the active and reactive power of the CS converter. The CS contains a BSS and five PHEVs of different ratings. Each of BSS and PHEV has a buck-boost converter that is controlled by aPID and a voltage regulator after the buck-boost converter as shown in Figure 2. The charging of BSS and PHEV takes place in buck mode and discharging takes place in boost mode. The BSS and each PHEV have a voltage regulator. The voltage regulator is controlled by the proposed adaptive FBL embedded FRANF-Leg-WC. The UG absorbs power in G2V mode during the time intervals of 10 to 12 h, 14 to 15 h, and 16 to 17 h. During these time intervals, different PHEVs are in discharging mode. The UG also absorbs power from BSS of CS in BSS2G mode during peak hours at the time interval of 18 to 22 h. In this duration, the BSS is in discharging mode. On the other hand, CS absorbs power from UG to entertain its BSS and PHEVs load. During time interval 1 to 2 h, the CS absorbs power from UG in G2BSS mode. Similarly, during the interval 4 to 5 h, the CS absorbs power from UG in G2V mode. V2V mode of operation occurs during

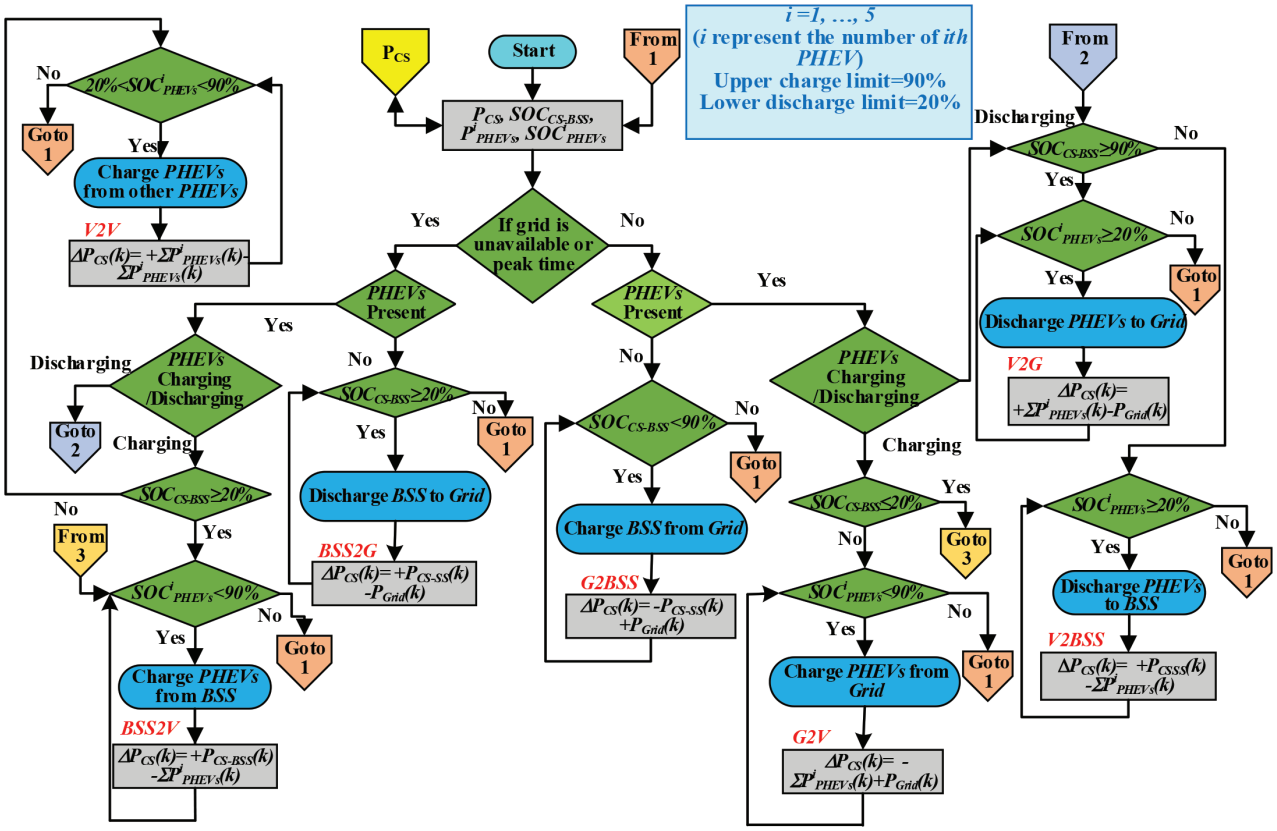

Figure 6. Flow chart of energy management system for charging station.

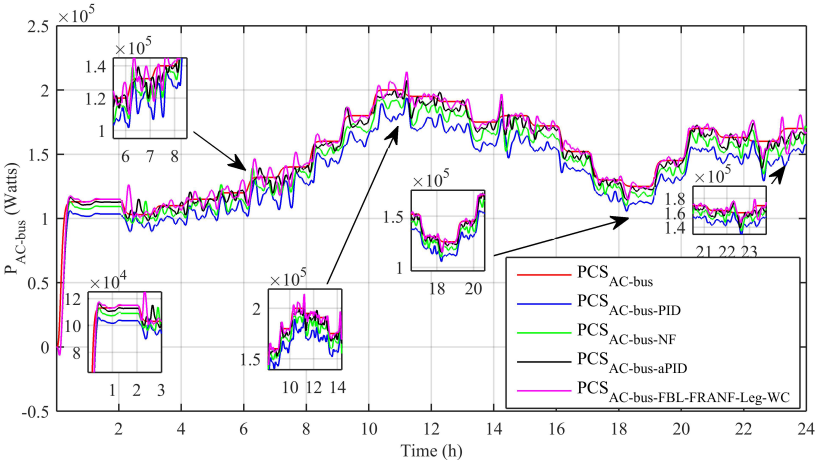

Figure 7. AC-bus active power.

interval 1 to 2 h, V2BSS mode of operation takes place during time interval 11 to 12 h, while BSS2V mode of operation occurs during 13 to 15 h. It is clear from Figure 9 and Figure 10 that the proposed adaptive FBL embedded FRANF-Leg-WC tracks the active and reactive power of CS's converter more efficiently as compared with adaptive NF, aPID, and PID control schemes.

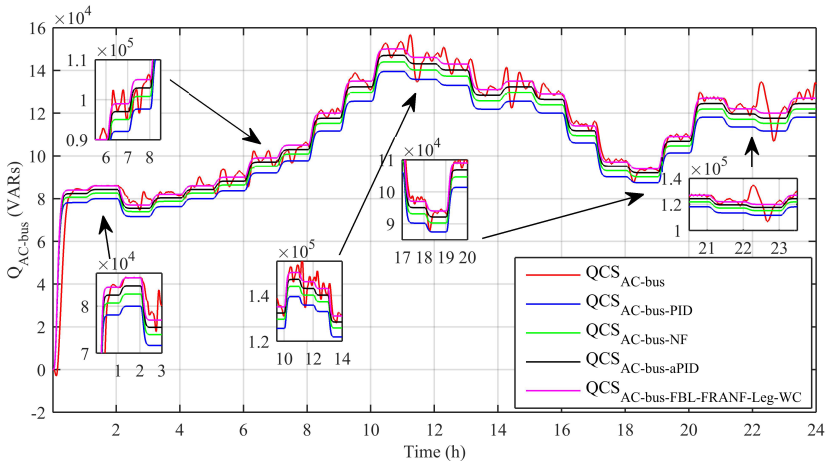

Figure 8. AC-bus reactive power.

The adaptive FBL embedded FRANF-Leg-WC gives steady state error = 0.0014 kW, overshoot = 0.4%, and undershoot = −0.1% in active power of CS. The aPID produces steady state error = 0.0289 kW, overshoot = 26.3%, and undershoot = −41.8% in active power of CS. The PID generates steady state error = 0.0027 kW, overshoot = 2.3%, and undershoot = −9% in active power of CS. The adaptive NF gives steady state error = 0.0662 kW, overshoot = 53.9%, and undershoot = −70.2% in active power of CS. The adaptive FBL embedded FRANF-Leg-WC generates steady state error = 0.09 kW, overshoot = 0.105%, and undershoot = −0.04% in reactive power of CS. The aPID produces steady state error = 0.1346 kW, overshoot = 11.2%, and undershoot = −28.4% in reactive power of CS. The PID produces steady state error = 0.1157 kW, overshoot = 4.6%, and undershoot = −5.6% in reactive power of CS. The adaptive NF gives steady state error = 0.1603 kW, overshoot = 14.8%, and undershoot = −22.3% in reactive power of CS.

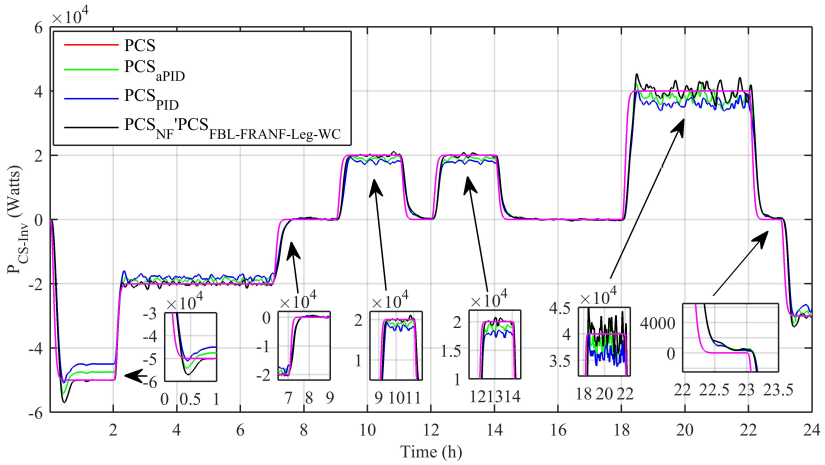

Figure 9. Charging station converter active power.

The SOC of a battery determines its mode of operation as a load and a source. Each PHEV and BSS in this research work is allowed to charge/discharge between specified limits, i.e., $20\% < SOC < 90\%$. Figure 11 shows that the BSS is in charge mode during time intervals 0 to 2 h and 11 to 12 h. During 0 to 2 h, the BSS is

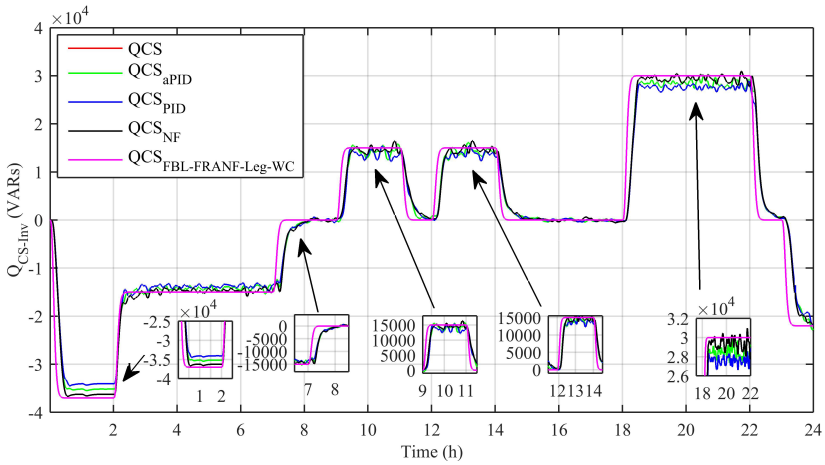

Figure 10. Charging station converter reactive power.

absorbing power from UG under the G2BSS mode of operation, while during 11 to 12 h, the BSS is absorbing power from PHEVs under V2BSS mode of operation. The BSS acts as a source during interval 13 to 15 h and 18 to 22 h and discharges to lower state of %SOC. The modes of operation are BSS2V and BSS2G respectively. Figure 12 shows the %SOC profile of PHEV-1 and depicts that the PHEV-1 is in charge mode during interval 1 to 2 h to charge %SOC under the V2V mode of operation, while it acts as a source and discharges during interval of 14 to 15 h under V2G mode of operation. Figure 13 shows the %SOC profile of PHEV-2 acting as a source and discharges during interval 1 to 2 h under the V2V mode of operation. Figure 14 shows the %SOC profile of PHEV-3 and reveals that it act as a load during interval 4 to 5 hour under G2V mode of operation. It acts as a source during interval 10 to 11 h and performs under V2G mode of operation. Figure 15 shows the %SOC profile of PHEV-4. It acts as a load during interval 4 to 5 h and charges under G2V mode of operation, while it acts as a source during 11 to 12 h and performs under V2G mode of operation. Figure 16 shows the %SOC profile of PHEV-5. This PHEV acts as a load from 13th to 14th h interval under BSS2V mode of operation, while it acts as a source from 16th to 17th h under V2G mode of operation.

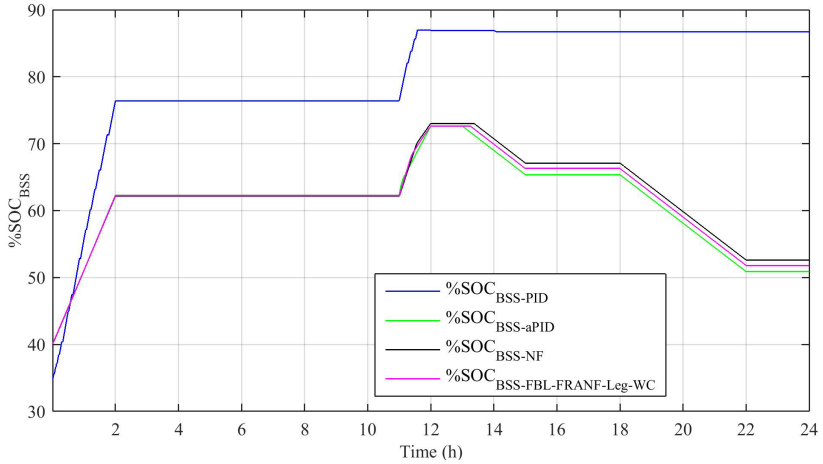

Figure 11. %SOC of BSS.

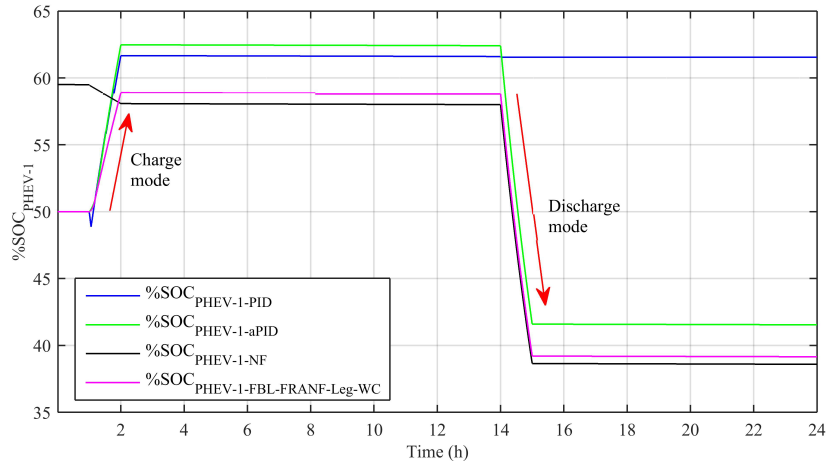

Figure 12. %SOC of PHEV-1.

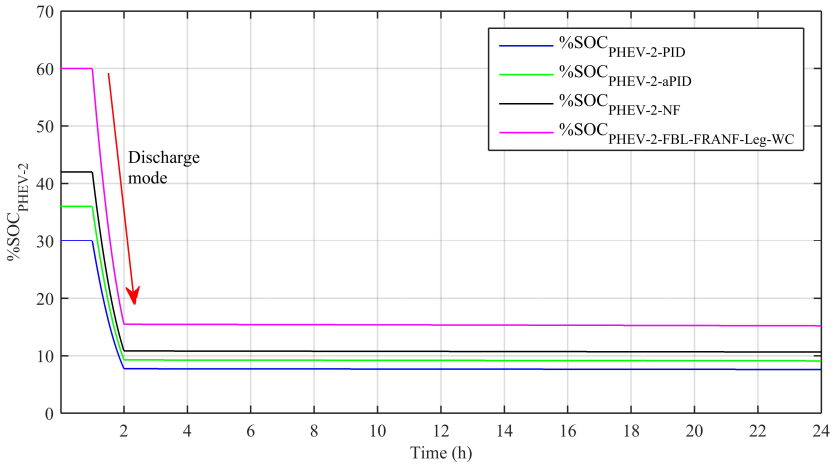

Figure 13. %SOC of PHEV-2.

Figure 17 shows the overall generation and consumption of power in the proposed MG-HPS during one complete solar day. All the RES are working on their MPPT and are controlled by aPID control scheme. It can be seen that overall load demand is fulfilled by the combined power generated from various RES. The storage system also absorbs power during off-peak hours, while it supplies power during peak-hours of operation. To ensure the power quality of microgrid, the $\%\Delta$THD content must be zero. Figure 18 shows the $\%\Delta$THD in load current of SMG-HPS. It is clear from the figure that $\%\Delta$THD produced by the proposed adaptive FBL embedded FRANF-Leg-WC almost flat as compared to adaptive NF, aPID and PID controls, thus, ensure more reliable operation of the power system. The content of $\%\Delta$f oscillations describes the power system stability. The lower magnitude of $\%\Delta$f shows the higher stability of the electric grid. Figure 19 shows the $\%\Delta$f in the load current. It is noteworthy that the $\%\Delta$ produced by proposed adaptive FBL embedded FRANF-Leg-WC is of much smaller value that adaptive NF, aPID and PID control schemes that improve power system stability. The $\%\Delta V_{RMS}$ is also a factor of power quality in the microgrid. Its lower magnitude guarantees the stable operation of the microgrid. Figure 20 shows the $\%\Delta V_{RMS}$ in load voltage profile. It shows that the minimum

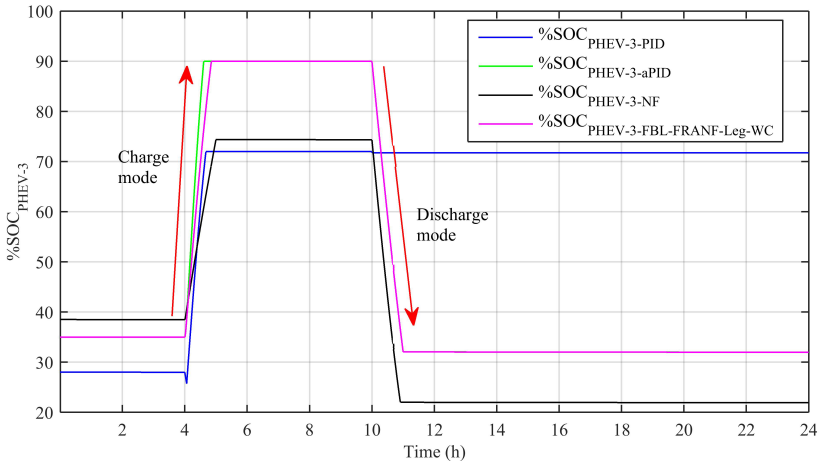

Figure 14. %SOC of PHEV-3.

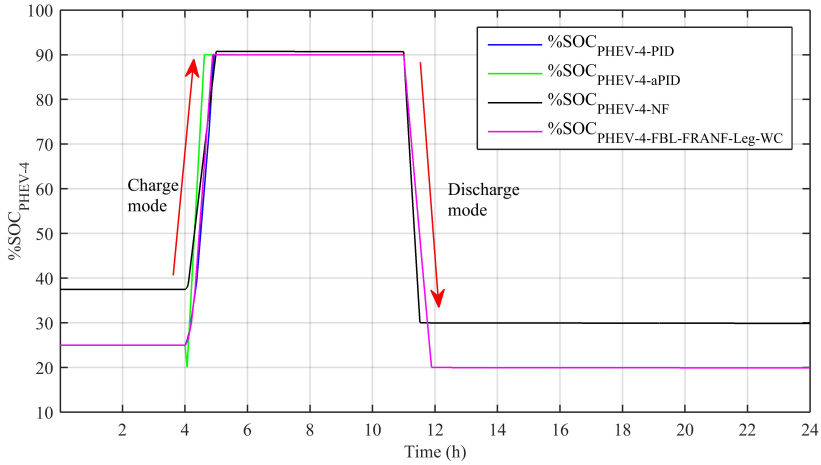

Figure 15. %SOC of PHEV-4.

Table 3. Power quality and power stability parameters.

Control scheme	%ΔTHD Absolute average	%ΔV_{RMS} Absolute average	%Δf Absolute average
PID	0.7524	0.4512	0.0002861
aPID	0.6493	0.4366	0.0030580
NF	0.5733	0.4249	0.0034290
FBL-FRANF-Leg-WC	0.5070	0.4086	0.0015160

fluctuation is produced by the suggested control scheme and, hence, shows its superior performance over aPID and PID controls. All the stability and quality parameters for MG-HPS are applied according to the IEEE standard 1547 [26]. The absolute average numerical values of power system stability and power quality are given in Table 3.

Figure 21(a) shows the estimated $\widehat{f}(x)$ and Figure 21(b) shows estimated $\widehat{g}(x)$ for all the PHEV's and

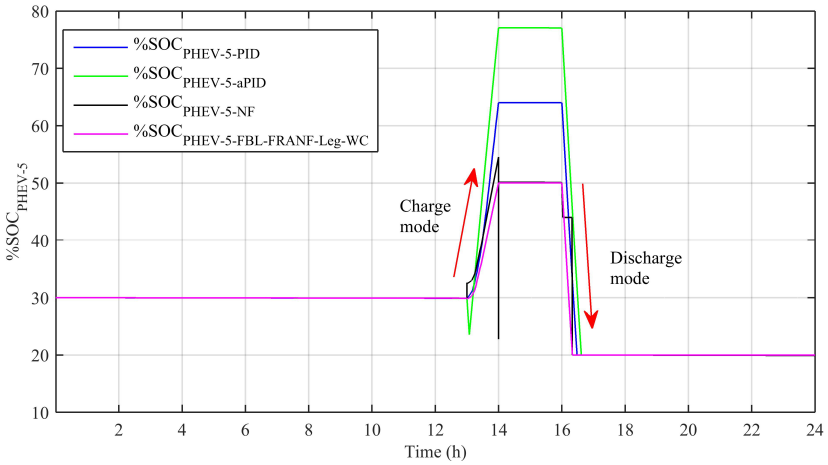

Figure 16. %SOC of PHEV-5.

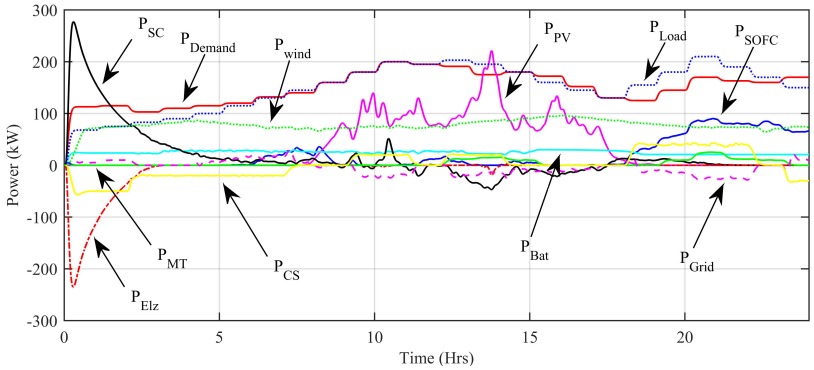

Figure 17. Generation and load power.

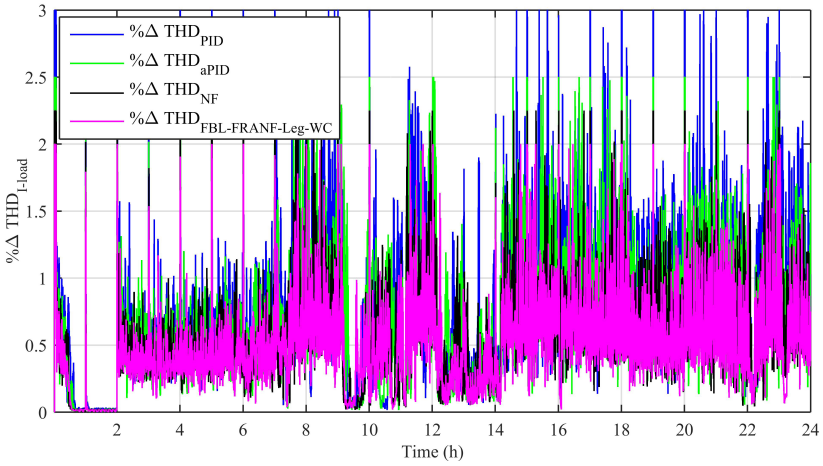

Figure 18. %ΔTHD in load current.

BSS. It is noteworthy that $\widehat{g}(x)$ should be greater than 0 due to its presence in denominator of (8. Therefore a saturator is used with lower limit of 0.01 to avoid division of zero. Figure 21(c) shows the plot of original signal

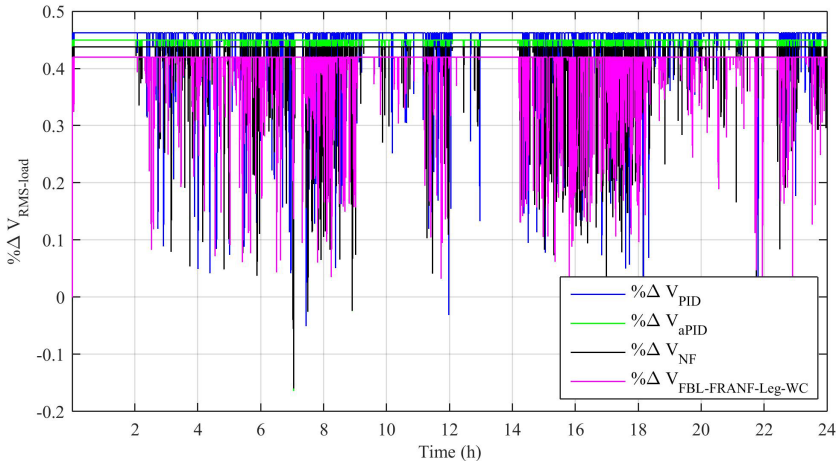

Figure 19. %Δf of load current.

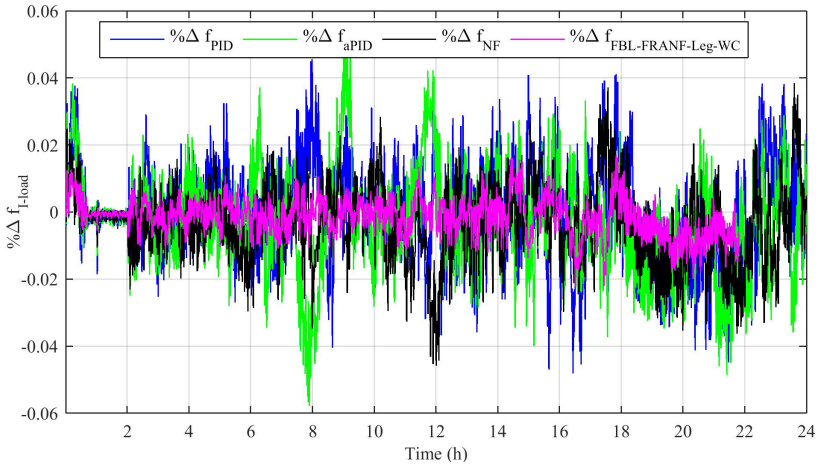

Figure 20. $\%\Delta V_{RMS}$ of load voltage.

$V_{PHEV} = y$ shown using red colour lines and identified signal $\widehat{f}(x) + \widehat{g}(x)u_{PHEV} = \widehat{y}$ shown using various colour. The results show that the PHEV's are successfully adopted online using the proposed control scheme and the nonlinear function are estimated correctly.

6. Conclusion

This article presents a grid-connected SMG-HPS having RES and MT as sources. RES are controlled by aPID for their MPPT. A CS is included in proposed SMG-HPS in which bidirectional power can flow under seven different scenarios. The proposed adaptive FBL embedded FRANF-Leg-WC is used to control the voltage regulator of each sub-component of CS. The performance of the stated scheme is tested for various tracking problems along with the reliability and stability of the power system. The %ΔTHD, and $\%\Delta V_{RMS}$, are minimized to ensure the application of power quality to the microgrid and %Δf is minimized to ensure the stability and smooth operation of the microgrid during various modes of operation. It is established that the performance of the proposed control schemes for all the scenarios is better than adaptive NF, conventional

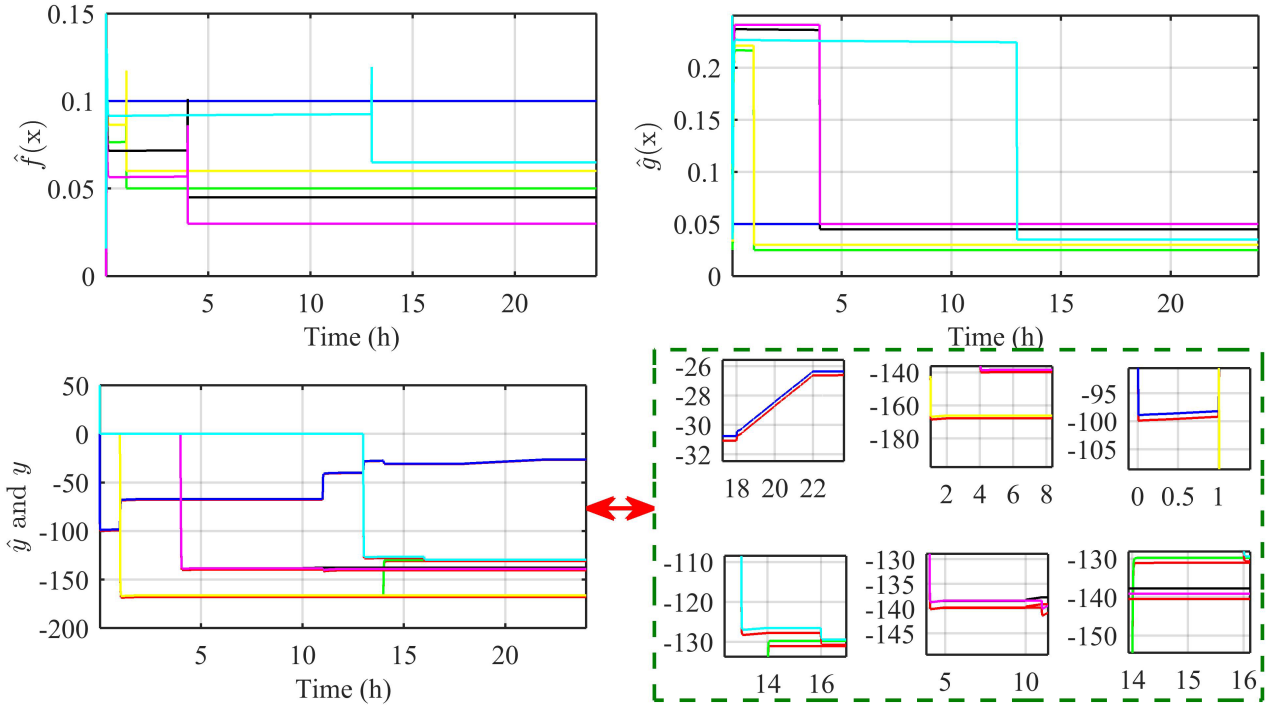

Figure 21. (a) $\widehat{f}(x)$ (b) $\widehat{g}(x)$ (c) $\widehat{y}$ and y.

aPID, and PID control schemes in terms of power quality, reference power tracking, and power system stability.

References

[1] Taghavipour A, Vajedi M, Azad NL. Intelligent control of connected plug-in hybrid electric vehicles. Cham, Switzerland AG: Springer, 2019. doi: 10.1007/978-3-030-00314-2.

[2] Ban D, Michailidis G, Devetsikiotis M. Demand response control for PHEV charging stations by dynamic price adjustments. In: IEEE 2012 PES Innovative Smart Grid Technologies Conference; Massachusetts Ave., NW Washington, DC, USA; 2012. pp. 1-8. doi: 10.1109/ISGT.2012.6175601.

[3] Mumtaz S, Ali S, Ahmad S, Khan L, Hassan SZ et al. Energy management and control of plug-In hybrid electric vehicle charging stations in a grid-connected hybrid power system. Energies 2017; 10 (11). doi: 10.3390/en10111923.

[4] Zhen Y, Bao Y, Zhong Z, Rinderknecht S, Zhou S. Development of a phev hybrid transmission for low-end mpvs based on amt. Vehicles 2020; 2 (2): 236-248. doi: 10.3390/vehicles2020013.

[5] Nafisi H, Agah SMM, Askarian Abyaneh H, Abedi M. Two-stage optimization method for energy loss minimization in microgrid based on smart power management scheme of phevs. IEEE Transactions on Smart Grid 2016; 7 (3): 1268-1276. doi: 10.1109/TSG.2015.2480999.

[6] Moeini-Aghtaie M, Abbaspour A, Fotuhi-Firuzabad M. Online multicriteria framework for charging management of phevs. IEEE Transactions on Vehicular Technology 2014; 63 (7): 3028-3037. doi: 10.1109/TVT.2014.2320963.

[7] Devaraj E, Joseph PK, Karuppa Raj Rajagopal T, Sundaram S. Renewable energy powered plugged-in hybrid vehicle charging system for sustainable transportation. Energies 2020; 13 (8). doi: 10.3390/en13081944.

[8] Malikopoulos AA. Supervisory power management control algorithms for hybrid electric vehicles: a survey. IEEE Transactions on Intelligent Transportation Systems 2014; 15 (5): 1869-1885. doi: 10.1109/ TITS.2014.2309674.

[9] Rahbari-Asr N, Chow M. Cooperative distributed demand management for community charging of phev/pevs based on kkt conditions and consensus networks. IEEE Transactions on Industrial Informatics 2014; 10 (3): 1907-1916. doi: 10.1109/TII.2014.230441210.1109/TII.2014.2304412.

[10] Faraji J, Abazari A, Babaei M, Muyeen SM, Benbouzid M. Day-ahead optimization of prosumer considering battery depreciation and weather prediction for renewable energy sources. Applied Sciences 2020; 10 (8). doi: 10.3390/app10082774.

[11] Kaur K, Dua A, Jindal A, Kumar N, Singh M, Vinel A. A novel resource reservation scheme for mobile phevs in v2g environment using game theoretical approach. IEEE Transactions on Vehicular Technology 2015; 64 (12): 5653-5666. doi: 10.1109/TVT.2015.2482462.

[12] Kreeumporn W, Ngamroo I. Optimal superconducting coil integrated into pv generators for smoothing power and regulating voltage in distribution system with phevs. IEEE Transactions on Applied Superconductivity 2016; 26 (7): 1-5. doi: 10.1109/TASC.2016.2591981.

[13] Hassan SZ, Kamal T, Riaz MH, Shah SAH, Ali HG et al. Intelligent control of wind-assisted phevs smart charging station. Energies 2019; 12 (5). doi: 10.3390/en12050909.

[14] Shafee S, Fotuhi-Firuzabad M, Rastegar M. Investigating the impacts of plug-in hybrid electric vehicles on power distribution systems. IEEE Transactions on Smart Grid 2013; 4 (3): 1351-1360. doi: 10.1109/TSG.2013.2251483.

[15] Pahasa J, Ngamroo I. Coordinated phev, pv, and ess for microgrid frequency regulation using centralized model predictive control considering variation of phev number. IEEE Access 2018; 6: 69151-69161. doi: 10.1109/ACCESS.2018.2879982.

[16] Pahasa J, Ngamroo I. PHEVs bidirectional charging/discharging and soc control for microgrid frequency stabilization using multiple mpc. IEEE Transactions on Smart Grid 2015; 6 (2): 526-533. doi: 10.1109/TSG.2014.2372038.

[17] Aragon-Aviles S, Trivedi A, Williamson SS. Smart power electronics-based solutions to interface solar-photovoltaics (pv), smart grid, and electrified transportation: state-of-the-art and future prospects. Applied Sciences 2020; 10 (14). doi: 10.3390/app10144988.

[18] Li S, Bao K, Fu X, Zheng H. Energy management and control of electric vehicle charging stations. Electric Power Components and Systems 2014; 42 (3-4): 339-347. doi: 10.1080/15325008.2013.837120.

[19] Clement-Nyns K, Haesen E, Driesen J. The impact of charging plug-in hybrid electric vehicles on a residential distribution grid. IEEE Transactions on Power Systems 2010; 25 (1): 371-380. doi: 10.1109/TPWRS.2009.2036481.

[20] Nguyen HNT, Zhang C, Mahmud MA. Optimal coordination of g2v and v2g to support power grids with high penetration of renewable energy. IEEE Transactions on Transportation Electrification 2015; 1 (2): 188-195. doi: 10.1109/TTE.2015.2430288.

[21] Haddadian G, Khalili N, Khodayar M, Shahidehpour M. Optimal scheduling of distributed battery storage for enhancing the security and the economics of electric power systems with emission constraints. Electric Power Systems Research 2015; 124: 152-159. doi: 10.1016/j.epsr.2015.03.002.

[22] Awais M, Khan L, Ahmad S, Mumtaz S, Badar R. Nonlinear adaptive NeuroFuzzy feedback linearization based MPPT control schemes for photovoltaic system in microgrid. PLOS ONE 2020; 15 (6): 1-36. doi: 10.1371/journal.pone.0234992.

[23] Lin X, Zhou K, Li H. AER adaptive control strategy via energy prediction for PHEV. IET Intelligent Transport Systems 2019; 13 (12): 1822-1831. doi: 10.1049/iet-its.2018.5582.

[24] Kamal T, Karabacak M, Hassan SZ, Fernandez-Ramirez LM, Riaz MH et al. Energy management and switching control of phev charging stations in a hybrid smart micro-grid system. Electronics 2018; 7 (9). doi: 10.3390/electronics7090156.

[25] Badar R, Khan L. Online adaptive legendre wavelet embedded neurofuzzy damping control algorithm. In: Proceedings of the 16th International Multi-Topic Conference; UET, Lahore, Pakistan. pp. 7-12. doi: 10.1109/INMIC.2013.6731316.

[26] IEEE standard for interconnection and interoperability of distributed energy resources with associated electric power systems interfaces. IEEE Std 1547-2018 (Revision of IEEE Std 1547-2003) 2018 April; 1-138. doi: 10.1109/IEEESTD.2018.8332112.